

Supernova Neutrino Opacity from Nucleon-Nucleon Bremsstrahlung and Related Processes

Steen Hannestad

Max-Planck-Institut für Physik (Werner-Heisenberg-Institut)

Föhringer Ring 6, 80805 München, Germany

and Theoretical Astrophysics Center, University of Aarhus, DK-8000 Aarhus C, Denmark

Georg Raffelt

Max-Planck-Institut für Physik (Werner-Heisenberg-Institut)

Föhringer Ring 6, 80805 München, Germany

ABSTRACT

Elastic scattering on nucleons, $\nu N \rightarrow N\nu$, is the dominant supernova (SN) opacity source for μ and τ neutrinos. The dominant energy- and number-changing processes were thought to be $\nu e^- \rightarrow e^- \nu$ and $\nu \bar{\nu} \leftrightarrow e^+ e^-$ until Suzuki (1993) showed that the bremsstrahlung process $\nu \bar{\nu} NN \leftrightarrow NN$ was actually more important. We find that for energy exchange, the related “inelastic scattering process” $\nu NN \leftrightarrow NN\nu$ is even more effective by about a factor of 10. A simple estimate implies that the ν_μ and ν_τ spectra emitted during the Kelvin-Helmholtz cooling phase are much closer to that of $\bar{\nu}_e$ than had been thought previously. To facilitate a numerical study of the spectra formation we derive a scattering kernel which governs both bremsstrahlung and inelastic scattering and give an analytic approximation formula. We consider only neutron-neutron interactions, we use a one-pion exchange potential in Born approximation, nonrelativistic neutrons, and the long-wavelength limit, simplifications which appear justified for the surface layers of a SN core. We include the pion mass in the potential and we allow for an arbitrary degree of neutron degeneracy. Our treatment does not include the neutron-proton process and does not include nucleon-nucleon correlations. Our perturbative approach applies only to the SN surface layers, i.e. to densities below about $10^{14} \text{ g cm}^{-3}$.

1. Introduction

A quantitatively accurate prediction of the fluxes and spectra of supernova (SN) neutrinos is required for a theoretical understanding of an array of fascinating phenomena, including the explosion mechanism itself, the cause of neutron star natal kicks, various aspects of SN nucleosynthesis, and the interpretation of the neutrino signal from SN 1987A and future galactic SNe, with or without the assumption of neutrino masses and mixings. However, at the present time one is far away from this goal because of numerical limitations and because of significant shortcomings in the calculation of the relevant microphysics, notably the equation of state and the neutrino opacities.

We presently study the opacity contribution of nucleon bremsstrahlung $NN \rightarrow NN\nu\bar{\nu}$ and its inverse $\nu\bar{\nu}NN \rightarrow NN$, processes which have been ignored in all numerical SN studies except for the proto-neutron star cooling calculations of Suzuki (1991, 1993) who found a significant modification of the neutrino fluxes and spectra. We also study the inelastic scattering process $\nu NN \rightarrow NN\nu$ which is obtained when crossing a final-state bremsstrahlung neutrino into the initial state. Janka et al. (1996) had stressed its apparent importance for the neutrino spectra formation, but without making a connection with Suzuki’s work. We will again motivate the importance of these processes and provide a scattering kernel which allows for a practical implementation in a numerical SN code. While this is a modest aspiration relative to the large number of open questions regarding SN neutrino opacities, we hope that our work may nevertheless prove useful for future numerical studies.

In order to appreciate the importance of nucleon bremsstrahlung and related reactions recall that for ν_e and $\bar{\nu}_e$ the dominant opacity contribution derives from charged-current processes (β processes) which involve electrons and positrons. In the diffusion regime they keep ν_e and $\bar{\nu}_e$ essentially in local thermal equilibrium. We are mostly concerned, however, with the transport of ν_μ , ν_τ , and their antiparticles, to which we will collectively refer as ν_μ . The dominant opacity contribution is the neutral-current scattering on nucleons $\nu_\mu N \rightarrow N\nu_\mu$, a process which does not equilibrate the neutrino number density and which is ineffective at modifying the spectrum because the neutrino energies are low relative to the mass of the nonrelativistic nucleons, especially in the outer layers of a SN core. Therefore, processes such as $\nu_\mu e^- \rightarrow e^- \nu_\mu$ and $\nu_\mu \bar{\nu}_\mu \leftrightarrow e^+ e^-$, which are subdominant with regard to the total opacity, are nevertheless important for the equilibration of the neutrino number density and spectra. It turns out that nucleon bremsstrahlung is far more effective than pair annihilation at equilibrating the neutrino number density, and it is of comparable importance to $\nu_\mu e^- \rightarrow e^- \nu_\mu$ at equilibrating the spectra. Moreover, the inelastic scattering process $\nu NN \rightarrow NN\nu$ is in turn far more effective at exchanging energy

than bremsstrahlung and is thus the dominant process for the neutrino spectra formation. Including these processes in a proto-neutron star cooling calculation would make the ν_μ spectrum far more similar to that of $\bar{\nu}_e$ than had been thought.

While nucleon bremsstrahlung and related processes are conceptually simple, a reliable calculation is nevertheless nontrivial. Difficulties include the nuclear matrix element, i.e. the appropriate nucleon-nucleon interaction potential, the intermediate degree of nucleon degeneracy, NN correlations, and the role of multiple-scattering effects. We will not be able to resolve all of these issues. For example, we will completely ignore NN correlations which may be quite important in some regions of the SN core where nuclei may not even be completely dissociated. In regions where nuclei exist, nuclear bound-bound or bound-free transitions involving neutral-current neutrino reactions may be important. The main advance of our calculation is the treatment of intermediate degrees of nucleon degeneracy in free-free transitions, the inclusion of the pion mass in the nucleon interaction potential, and the inclusion of multiple-scattering effects. Our scattering kernel is then self-consistent in the sense that it allows for the simultaneous treatment of bremsstrahlung and inelastic scattering while producing the correct total νN scattering cross section.

We focus on the neutrino spectra formation which takes place in the surface layers of a proto neutron star where number-equilibrating, energy-equilibrating, and finally scattering processes freeze out at different radii so that the different neutrino species are emitted with different fluxes and different spectral temperatures, but approximately equal luminosities. We expect that bremsstrahlung and inelastic scattering make the spectra and fluxes more similar than had been thought previously.

Nucleon-nucleon interactions not only lead to bremsstrahlung and the inelasticity of neutrino-nucleon scattering, but also to a reduction of the overall νN scattering cross section (Raffelt & Seckel 1995; Sawyer 1995; Raffelt, Seckel & Sigl 1996). This cross-section reduction is an inevitable consequence of the fact that nucleon spins interact so that one cannot consistently include bremsstrahlung and the inelasticity of νN scattering and yet ignore this cross-section reduction. Unfortunately, for densities above, say, $10^{14} \text{ g cm}^{-3}$ a controlled calculation of the scattering kernel and thus of the neutrino transport coefficients is currently out of reach. The only hint as to the possible magnitude of the cross-section reduction in the inner parts of a SN core derives from the signal duration of SN 1987A (Keil, Janka & Raffelt 1995) and the f -sum rule of the spin-density structure function (Sigl 1996) which imply that a naive extrapolation of the perturbative spin-density structure function into the high-density regime would significantly overestimate the cross-section suppression. Recent 2-dimensional hydrodynamic SN cooling calculations indicate that actually convection, not neutrino radiative transport, may be the dominant mode of energy

transfer from the inner proto-neutron star to the neutrino sphere (Keil, Janka & Müller 1996), rendering the high-density opacities less critical for the overall neutrino luminosity. In any case, the problem of the neutrino spectra formation in the surface layers is rather disjoint from the problem of calculating the overall neutrino luminosity.

We begin our discussion in Sec. 2 with a comparison of the different neutrino opacity contributions and thus motivate the importance of nucleon bremsstrahlung and related processes. In Sec. 3 we formulate the bremsstrahlung rate in terms of the dynamical spin-density structure function (the scattering kernel) and thus reduce the problem to the calculation of a dimensionless function which includes all of the nuclear and many-body complications. We also discuss the underlying nuclear matrix element of the bremsstrahlung process. In Sec. 4 we study the nucleon phase space and provide the appropriate analytic approximation formulae. In Sec. 5 we summarize and discuss our results.

2. Comparison of Opacity Sources

2.1. Mean Free Path

In a SN core the main opacity source for μ and τ neutrinos is neutral-current scattering on nucleons. However, the large nucleon mass relative to typical neutrino energies renders this process ineffective at equilibrating the neutrino spectra and it certainly cannot modify the neutrino number density. We begin with a comparison of the relative importance of those processes which are subdominant with regard to the total opacity, yet allow for an effective modification of the ν_μ spectrum and density. The simplest case is $\nu_\mu\bar{\nu}_\mu \rightarrow \nu_e\bar{\nu}_e$. Using Maxwell-Boltzmann distributions at temperature T for all neutrino species, we find the thermally averaged absorption rate

$$\Gamma_0 \equiv \frac{4}{\pi^3} G_F^2 T^5, \quad (1)$$

which sets a natural scale for all other processes. We use natural units with $\hbar = c = k_B = 1$. The rate for $\nu_\mu\nu_e \rightarrow \nu_\mu\nu_e$ together with that for $\nu_\mu\bar{\nu}_e \rightarrow \nu_\mu\bar{\nu}_e$ is $4\Gamma_0$. For $\nu_\mu\bar{\nu}_\mu \rightarrow e^+e^-$ it is $\Gamma_0(C_{V,e}^2 + C_{A,e}^2)\eta_e^4 e^{-\eta_e}/12$ while it is $\Gamma_0(C_{V,e}^2 + C_{A,e}^2)3\eta_e^2$ for $\nu_\mu e^\pm \rightarrow \nu_\mu e^\pm$, where $\eta_e \gg 1$ is the electron degeneracy parameter. The weak coupling constants are $C_{A,e} = -\frac{1}{2}$ and $C_{V,e} = -\frac{1}{2} + 2\sin^2\Theta_W$ for ν_μ and ν_τ . Neutrino coalescence $\nu\bar{\nu} \rightarrow$ plasmon is negligible. Finally, there is inverse bremsstrahlung on nucleons $\nu_\mu\bar{\nu}_\mu NN \rightarrow NN$; the spectrally averaged absorption rate is given by Eq. (25) in Sec. 3.4.

In order to compare these different processes for realistic conditions we use the numerical SN model S2BH_0 of Keil, Janka & Raffelt (1995) which represents a SN core

1 s after collapse; the radial profiles of various physical parameters are shown in Fig. 1. In the outer parts of the star, which is where the neutrino spectra are formed, the effective nucleon degeneracy parameter $\eta_* = p_F^2/2m_N T$ varies between 2 and 4, η_e between 1 and 8, and the range of relevant temperatures is taken to be $T = 5\text{--}10$ MeV, leading to

$$\Gamma = \Gamma_0 \times \begin{cases} 0.03\text{--}0.4 & \text{for } \nu_\mu \bar{\nu}_\mu \rightarrow e^+ e^-, \\ 1 & \text{for } \nu_\mu \bar{\nu}_\mu \rightarrow \nu_e \bar{\nu}_e, \\ 4 & \text{for } \nu_\mu \nu_e \rightarrow \nu_\mu \nu_e \text{ plus } \nu_\mu \bar{\nu}_e \rightarrow \nu_\mu \bar{\nu}_e, \\ 2\text{--}50 & \text{for } \nu_\mu e^+ \rightarrow \nu_\mu e^+ \text{ plus } \nu_\mu e^- \rightarrow \nu_\mu e^-, \\ 15\text{--}300 & \text{for } \nu_\mu \bar{\nu}_\mu nn \rightarrow nn. \end{cases} \quad (2)$$

We conclude that for typical SN conditions bremsstrahlung is by far the most important number-changing reaction. Even for energy exchange it is more important than elastic scattering on electrons and positrons.

2.2. Energy Transfer

The processes considered in the previous section are very effective at transferring energy in the sense that in a given interaction the neutrino essentially loses all memory of its previous energy. This is not the case for the “inelastic scattering process” $\nu nn \rightarrow nn\nu$ which is the bremsstrahlung process with a final-state neutrino crossed into the initial state. While we use the term “inelastic scattering process” we stress that it is not logically distinct from the “elastic channel” $\nu n \rightarrow n\nu$. Both are described by one and the same scattering kernel which has a finite width as a function of the energy transfer ω due to the nucleon-nucleon interaction. Therefore, in each collision the final-state neutrino energy is smeared out by a small amount which is given by the width of the scattering kernel.

To quantify the efficiency of energy transfer of this process relative to those of the previous section it is useful to consider a fluid of neutrinos at a temperature T_ν which is slightly different than the temperature T of the neutron bath. According to Eqs. (31) and (34) we find for the rate of energy transfer between these fluids

$$\frac{\Delta Q}{\Delta T} = \frac{3C_A^2 G_F^2 n_B T^5}{\pi^3} \frac{\Gamma_\sigma}{2\pi T} \times \begin{cases} 1 & \text{for } nn \leftrightarrow nn\nu\bar{\nu}, \\ 20 & \text{for } \nu nn \leftrightarrow nn\nu, \end{cases} \quad (3)$$

where the spin-fluctuation rate Γ_σ is given in Eq. (20). For the bremsstrahlung case we have included a factor 1/2 relative to Eq. (31); we only count the energy transferred to the neutrinos. These results receive numerical corrections of order unity for realistic conditions, reducing the relative importance of scattering to perhaps a factor of 10.

For completeness we have calculated the same quantity for neutrino scattering on degenerate electrons,

$$\frac{\Delta Q_{\nu e^- \leftrightarrow e^- \nu}}{\Delta T} = \frac{24}{\pi^5} G_F^2 (C_{V,e}^2 + C_{A,e}^2) \eta_e^2 T^8, \quad (4)$$

where again $C_{V,e} \approx 0$ and $C_{A,e} = -\frac{1}{2}$ for ν_μ . Relative to inelastic nucleon scattering this is

$$\frac{\Delta Q_{\nu_\mu e^- \leftrightarrow e^- \nu_\mu}}{\Delta Q_{\nu_\mu nn \leftrightarrow nn \nu_\mu}} = 1.37 \times 10^{-3} \frac{\eta_e^2}{\eta_*^3} T_{10}^{1/2}, \quad (5)$$

where $T_{10} = T/10$ MeV. In the outer part of our SN model we have $\eta_e < 8$, $\eta_* = 2-4$, and $T_{10} = 0.5-1$ so that the ratio is always smaller than 0.01. Electrons are negligible for the energy transfer, in complete keeping with the conclusions of Janka et al. (1996).

In the calculation of bremsstrahlung and related processes we assume nonrelativistic nucleons and use the long-wavelength approximation. As a consequence neutrinos cannot transfer energy to the nucleons if the NN interaction is switched off. From Janka (1991) and Tubbs (1979) and using a Maxwell-Boltzmann distribution for the neutrinos we find

$$\frac{\Delta Q_{\text{recoil}}}{\Delta T} = \frac{(C_V^2 + 5C_A^2) G_F^2 n_B T^5}{\pi^3} \frac{240 T}{m_N}. \quad (6)$$

Naturally, the vector-current interaction appears here in contrast to bremsstrahlung-related effects. Ignoring C_V^2 we find

$$\frac{\Delta Q_{\nu nn \leftrightarrow nn \nu}}{\Delta Q_{\text{recoil}}} = \frac{m_N \Gamma_\sigma}{40\pi T^2} = \alpha_\pi^2 \frac{2\sqrt{2}\pi}{15\pi^3} \eta_*^{3/2} = 1.21 \eta_*^{3/2}, \quad (7)$$

where we have used Eq. (20) for the spin-fluctuation rate. The vector current contribution to recoils reduces this ratio a bit, and pion-mass effects reduce the inelastic term by another small amount so that it may be more realistic to take something like $0.5 \eta_*^{3/2}$. In the SN core model of Fig. 1 we always have $\eta_* = 2-4$ so that recoil effects are always of roughly equal importance to inelastic scattering. Therefore, the transfer of energy is even more effective than what is accounted for by our scattering kernel which ignores nucleon recoils.

2.3. Energy Sphere

We may next attempt to estimate the change in the spectral temperature of the emitted neutrino fluxes which is brought about by including bremsstrahlung and related processes. Neutrinos stream off freely from the “transport sphere” which is the radius where scattering on nucleons is no longer effective at trapping them. Deeper inside is the “energy sphere” which is the radius where energy-exchanging processes such as scattering

on electrons become ineffective (Burrows & Mazurek 1982, 1983). We presently estimate the temperature of the energy sphere for the SN model of Fig. 1 with or without the inclusion of bremsstrahlung and inelastic scattering. We take the change in this temperature as an indication of the changed spectral temperature of the emitted neutrinos. We stress, of course, that the temperature at the energy sphere is not identical with the spectral temperature of the emitted neutrino flux which is modified by the fact that lower energy neutrinos diffuse more effectively through the layer between the energy and the transport spheres. Still, we think that the following procedure gives one a sense of the quantitative importance of bremsstrahlung and its sister reactions.

In order to calculate the location of the energy sphere we introduce the effective mean free path for energy exchange (Shapiro & Teukolsky 1983)

$$\lambda_{\text{eff}}^{-1} = \sqrt{\lambda_{\text{tot}}^{-1} \lambda_e^{-1}}. \quad (8)$$

Here, λ_{tot} is the mean free path for a neutrino of a given energy while λ_e is the mean free path against energy-changing reactions. If energy-changing reactions dominate the total opacity we have $\lambda_{\text{tot}} \simeq \lambda_e$ and thus $\lambda_{\text{eff}} \simeq \lambda_e$. However, in a “scattering atmosphere” as in a SN core where $\lambda_{\text{tot}} \simeq \lambda_{\text{scatter}}$ the trapping of neutrinos by collisions gives them a larger chance to lose energy by some other process, leading to an increased value of $\lambda_{\text{eff}}^{-1}$ relative to λ_e^{-1} . We define the radius R_e of the energy sphere by

$$\int_{R_e}^{\infty} dr \lambda_{\text{eff}}^{-1} = \frac{2}{3}, \quad (9)$$

i.e. by the radius where the effective optical depth is $\frac{2}{3}$.

We have performed this calculation for the SN model of Fig. 1 first for muon neutrinos by including the neutral-current scattering on protons and neutrons as the dominant scattering process. Nucleon degeneracy effects were taken into account. As an energy-exchange process we first use electron scattering, again including degeneracy effects. We then find that the temperature of the energy sphere varies with neutrino energy as shown by the solid line in Fig. 2. Next we use inverse bremsstrahlung as the only energy-changing reaction according to the numerical prescription developed in Sec. 4, leading to the short-dashed line. We see that the two processes are of roughly equal importance, with electron scattering dominating for relatively large neutrino energies. We have repeated the same exercise for $\bar{\nu}_e$, except that we include the charged-current reaction $\bar{\nu}_e p \rightarrow n e^+$ as an energy-changing reaction, leading to the long-dashed curve. Evidently this is the most important reaction for $\bar{\nu}_e$ and thus dominates the spectrum formation.

To extract one fixed energy-sphere radius we next take neutrinos to be in thermal equilibrium up to their energy sphere so that their distribution is characterized by the local

medium temperature, and that further out they are characterized by their energy-sphere temperature. All reaction rates are averaged with this spectral distribution so that

$$\langle \lambda_{\text{eff}}^{-1} \rangle = \sqrt{\langle \lambda_{\text{tot}}^{-1} \rangle \langle \lambda_e^{-1} \rangle}. \quad (10)$$

The energy sphere is defined as in Eq. (9) except using $\langle \lambda_{\text{eff}}^{-1} \rangle$ instead of $\lambda_{\text{eff}}^{-1}$. In order to locate the neutrino sphere we must now perform an iteration, assuming first some estimate for the energy-sphere temperature to determine the location where the effective optical depth is $\frac{2}{3}$, then use the temperature there as the next approximation, and so forth until convergence (Keil & Janka 1995). We stress that our benchmark model was calculated with equilibrium neutrino transport everywhere so that it becomes actually more self-consistent, not less so, when the neutrinos are kept in equilibrium out to larger radii.

For the SN core model of Fig. 1 we find the energy-sphere temperatures and densities shown in Table 1. We have included the bremsstrahlung process according to the prescription developed in Secs. 3 and 4, and then multiplied its rate by a factor f_{brems} . For $f_{\text{brems}} = 0$ we find the energy sphere without bremsstrahlung while $f_{\text{brems}} = 1$ includes the full effect. We also show the redshifted energy-sphere temperatures for an observer at infinity and the total optical depth at the location of the energy sphere, again for a spectrally averaged neutrino mean free path. We are thus led to conclude that bremsstrahlung alone reduces the ν_μ spectral temperature by about 1 MeV, while that of $\bar{\nu}_e$ remains largely unchanged. The change of the ν_μ spectrum agrees with Suzuki’s (1991, 1993) results.

In order to estimate the impact of inelastic scattering we recall that it is by a factor of 10 more important than bremsstrahlung, give or take a factor of 2. Therefore, we have also calculated the energy sphere for $f_{\text{brems}} = 5, 10, \text{ and } 20$, which probably mimics the effect of inelastic scattering and its uncertainty. The $\bar{\nu}_e$ temperature is still only mildly affected, suggesting that β processes are still very important for this species. The ν_μ temperature is significantly lowered; it is very close to that of $\bar{\nu}_e$.

Of course, including NN interactions consistently will probably accelerate the cooling process due to the reduced overall neutrino scattering cross section in the deep interior of the SN core. This will likely heat the neutrino sphere so that the spectral temperatures may actually *increase*. A similar effect will be caused by convection if it is a generic phenomenon for the proto-neutron star evolution. We believe, however, that our schematic treatment gives us a reasonable estimate of the *differential* temperature change, i.e. the ν_μ and $\bar{\nu}_e$ temperatures will be much closer than is often assumed.

A quantitative assessment of the spectral modifications requires detailed numerical simulations which we are in no position to perform. In the following, however, we provide a scattering kernel which is needed for such an investigation.

3. Bremsstrahlung and Related Processes

3.1. Scattering Kernel

For a numerical study the bremsstrahlung process, its inverse, and inelastic scattering are best formulated in terms of a “scattering kernel” which contains all of the properties of the nuclear medium, but which excludes the neutrino phase-space integration. We begin with the usual weak interaction Hamiltonian density¹

$$\mathcal{H}_{\text{int}} = \frac{G_F}{\sqrt{2}} \bar{\psi}_N \gamma_\mu (C_V - C_A \gamma_5) \psi_N \bar{\psi}_\nu \gamma_\mu (1 - \gamma_5) \psi_\nu \quad (11)$$

where G_F is Fermi’s constant, ψ_N the nucleon Dirac field for either protons or neutrons, and ψ_ν the neutrino field. The neutral-current vector coupling constant is $\frac{1}{2} - 2 \sin^2 \Theta_W \approx 0$ for protons and $-\frac{1}{2}$ for neutrons. The axial-current coupling is often taken to be $\pm 1.26/2$ for protons and neutrons, respectively, but the strange-quark contribution to the nucleon spin causes certain deviations from this simple picture (Raffelt & Seckel 1995).

We are concerned with conditions where the temperature is below 10 MeV so that a typical nucleon velocity is around $0.2c$. Therefore, it is reasonable to use the nonrelativistic limit which implies that only the axial vector current contributes to bremsstrahlung (Friman & Maxwell 1979; Raffelt & Seckel 1995). The squared matrix element for the emission of a neutrino pair, $N_1 + N_2 \rightarrow N_3 + N_4 + \nu + \bar{\nu}$, may be written as

$$\sum_{\text{spins}} |\mathcal{M}|^2 = \left(\frac{C_A G_F}{\sqrt{2}} \right)^2 M_{\mu\nu} N^{\mu\nu}, \quad (12)$$

where $M^{\mu\nu}$ and $N^{\mu\nu}$ stand for the nucleonic and neutrino parts, respectively. From the discussion in Raffelt and Seckel (1995) it follows that in an isotropic medium and for nonrelativistic nucleons it is enough to consider the spatial trace $\bar{M} \equiv \frac{1}{3} M_i^i$ which defines the “reduced squared matrix element.” Equation (12) may thus be written as

$$\sum_{\text{spins}} |\mathcal{M}|^2 \rightarrow \left(\frac{C_A G_F}{\sqrt{2}} \right)^2 \bar{M} 8\omega_1 \omega_2 (3 - \cos \theta), \quad (13)$$

where $\omega_{1,2}$ are the neutrino energies and θ is the angle between their momenta. With these simplifications and in the long-wavelength limit the scattering kernel is

$$S_\sigma^{(1)}(\omega) = \frac{1}{n_B} \int \prod_{i=1}^4 \frac{d^3 \mathbf{p}_i}{2m_N (2\pi)^3} f_1 f_2 (1 - f_3) (1 - f_4) \bar{M} \\ \times (2\pi)^4 \delta(E_1 + E_2 - E_3 - E_4 + \omega) \delta^3(\mathbf{p}_1 + \mathbf{p}_2 - \mathbf{p}_3 - \mathbf{p}_4), \quad (14)$$

¹In previous papers (e.g. Janka et al. 1996) it had been written $(G_F/2\sqrt{2}) \dots$ so that, for example, C_A was ± 1.26 rather than $\pm 1.26/2$ which we use here.

where n_B is the baryon density. Further, f_i is the occupation number of nucleon i with energy E_i and momentum \mathbf{p}_i while $\omega = -(\omega_1 + \omega_2)$ for pair emission and $\omega = \omega_1 + \omega_2$ for pair absorption, i.e. ω is the transfer of energy to the nuclear medium. For neutron-neutron or proton-proton bremsstrahlung we need to include a statistics factor 1/4 to compensate for initial- and final-state double counting. The superscript (1) signifies that in this form the scattering kernel is a lowest-order perturbative result, derived from a bremsstrahlung calculation. The subscript σ indicates that in the framework of linear-response theory it is the nucleon spin-density autocorrelation function (e.g. Janka, Keil, Raffelt & Seckel 1996). Both the lowest order $S_\sigma^{(1)}(\omega)$ and the full spin-density autocorrelation function $S_\sigma(\omega)$ obey detailed balance $S_\sigma(-\omega) = S_\sigma(\omega) e^{-\omega/T}$.

In our treatment we always assume that the neutron spins evolve independently of each other, i.e. we ignore possible spin-spin correlations. In this case the full scattering kernel must obey the normalization requirement (Raffelt & Strobel 1997)

$$\int_{-\infty}^{+\infty} \frac{d\omega}{2\pi} S_\sigma(\omega) = \frac{1}{n_B} \int \frac{2d^3\mathbf{p}}{(2\pi)^3} f_p(1 - f_p) \equiv B \quad (15)$$

where f_p is the occupation number of a neutron with momentum \mathbf{p} and the factor 2 represents the two spin orientations. In the nondegenerate case where we may neglect the Pauli blocking factor $(1 - f_p)$ the normalization is unity.

3.2. Nuclear Matrix Element

3.2.1. Identical Nucleons

In order to calculate the scattering kernel we need to know the nuclear matrix element. The bremsstrahlung emission of neutrino pairs or axions arises from nucleon spin fluctuations in collisions so that one needs a spin-dependent nucleon-nucleon potential. The most general velocity-independent interaction has a scalar (spin-independent) part, a central part proportional to $\boldsymbol{\sigma}_1 \cdot \boldsymbol{\sigma}_2$, and a tensor part proportional to $3\hat{\mathbf{r}} \cdot \boldsymbol{\sigma}_1 \hat{\mathbf{r}} \cdot \boldsymbol{\sigma}_2 - \boldsymbol{\sigma}_1 \cdot \boldsymbol{\sigma}_2$ where $\boldsymbol{\sigma}_{1,2}$ are the spin operators of the two nucleons (Blatt & Weisskopf 1979, Ericson & Weise 1988). These interactions have the important property that they conserve the square of the total nucleon spin, i.e. $(\boldsymbol{\sigma}_1 + \boldsymbol{\sigma}_2)^2$ is a constant of the motion. In addition, the scalar and central parts conserve the total spin $(\boldsymbol{\sigma}_1 + \boldsymbol{\sigma}_2)$.

We first consider bremsstrahlung from the collision of identical nucleons (proton-proton or neutron-neutron collisions). The emission of neutrino pairs or axions is induced by the total spin operator $(\boldsymbol{\sigma}_1 + \boldsymbol{\sigma}_2)$ which evolves nontrivially only due to the tensor interaction. Because the physical cause of the tensor interaction is primarily one-pion exchange (OPE)

one expects that an OPE ansatz captures the dominant aspect of the bremsstrahlung process (Friman & Maxwell 1979). In addition, the spin operator has nonvanishing matrix elements only between triplet states. Because the total wavefunction must be antisymmetric the orbital angular momentum of the relevant states must be odd. Therefore, s -waves do not contribute so that the least well-known short-distance part of the nucleon interaction potential does not affect the nucleon motion, further justifying the OPE ansatz.

For identical nucleons the OPE squared matrix element in its “reduced form” is found to be (Raffelt & Seckel 1995)

$$\overline{M} = \frac{64(4\pi)^2}{3} \frac{\alpha_\pi^2}{\omega^2} \left[\left(\frac{\mathbf{q}^2}{\mathbf{q}^2 + m_\pi^2} \right)^2 + \left(\frac{\mathbf{q}_*^2}{\mathbf{q}_*^2 + m_\pi^2} \right)^2 + \frac{\mathbf{q}^2 \mathbf{q}_*^2 - 3(\mathbf{q} \cdot \mathbf{q}_*)^2}{(\mathbf{q}^2 + m_\pi^2)(\mathbf{q}_*^2 + m_\pi^2)} \right], \quad (16)$$

where $\omega = E_4 + E_3 - E_2 - E_1$ is the energy transfer to the nucleons, $\mathbf{q} = \mathbf{p}_2 - \mathbf{p}_4$ is the momentum transfer between the nucleons, and $\mathbf{q}_* = \mathbf{p}_2 - \mathbf{p}_3$ the momentum transfer for the exchange amplitude. Further, $\alpha_\pi \equiv (f^2 m_N / m_\pi)^2 / 4\pi \approx 15$ with $f \approx 1$ is the pion-nucleon “fine-structure constant.”

At a temperature T a typical nucleon momentum is $(3m_N T)^{1/2}$ so that a typical momentum exchange in a collision is of a similar magnitude. At $T = 10$ MeV this is about 170 MeV, only slightly larger than the pion mass of 135 MeV. First, this implies that the pion mass cannot be ignored in the denominators in Eq. (16). Secondly, it means that the typical potential region probed is not much smaller than m_π^{-1} so that, again, the OPE potential should be a reasonable approximation.

Two-pion exchange effects become important at distances below $2 \text{ fm} \simeq 1.5 m_\pi^{-1}$ (Ericson & Weise 1988). Their impact on the bremsstrahlung process can be estimated by mimicking the two-pion exchange contribution by one- ρ -meson exchange where the mass of this effective particle is taken to be $m_\rho \approx 600$ MeV. A typical term in Eq. (16) is then modified to (Ericson & Mathiot 1989)

$$\left(\frac{\mathbf{q}^2}{\mathbf{q}^2 + m_\pi^2} \right)^2 \rightarrow \left(\frac{\mathbf{q}^2}{\mathbf{q}^2 + m_\pi^2} - C_\rho \frac{\mathbf{q}^2}{\mathbf{q}^2 + m_\rho^2} \right)^2 \quad (17)$$

with $C_\rho = 1.67$. Taking \mathbf{q}^2 to be $3Tm_N$ with $T = 10$ MeV, i.e. taking $|\mathbf{q}|$ to be around 170 MeV yields a 35% reduction of the squared matrix element. This estimate quantifies the error one is likely to make by using a simple OPE potential.

Even if the OPE potential is taken to be appropriate, this alone does not guarantee that the Born approximation is justified which was used to calculate Eq. (16). Ericson & Weise (1988) compare the p -wave scattering volumes of an OPE Born calculation with an iterated OPE calculation and with a full calculation using the Paris nucleon-nucleon potential. The

OPE Born approximation, again, yields a certain overestimate so that for our conditions of interest the correct result may be smaller by as much as 50%. These uncertainties set the scale of precision that one may hope to achieve with our simple approach.

The OPE approximation may be tested by comparing the calculated rate for the pionic bremsstrahlung process $pp \rightarrow pp\pi^0$ with experimental data (Choi, Kang & Kim 1989; Turner, Kang & Steigman 1989). The pion coupling is of derivative nature so that only the axial-vector current contributes, rendering this process a good proxy for the bremsstrahlung emission of neutrino pairs. However, because of the pion mass threshold the kinematical regime probed is always at higher (but not very much higher) energies than what is appropriate for a SN core, and one needs to include relativistic corrections which are no longer negligible. The agreement between an OPE calculation and the data found by Turner, Kang & Steigman (1989) is far better than one would have expected according to our above caveats. After all, one now probes the NN interaction potential at distances where two-pion exchange and other corrections surely must be important. This example illustrates the well-known fact that the OPE potential in Born approximation often yields far better results for spin-dependent processes than one is entitled to expect.

3.2.2. Proton-Neutron Scattering

The situation is far more complicated for proton-neutron scattering. Because the neutrino neutral-current coupling to protons and neutrons is nearly equal but of opposite sign, the pair emission is now induced essentially by the operator $\sigma_1 - \sigma_2$ which is not conserved by the central part of the interaction potential. This operator connects triplet and singlet states, i.e. the selection rules of the neutron-neutron system do not apply. Further, the two-nucleon wave function can be antisymmetric in the isospin variables so that orbital s -waves allow for both singlet and triplet states. Put another way, the short-distance behavior of the potential does matter in this context. By the same token, the comparison of Turner, Kang & Steigman (1989) with experimental data is not directly relevant.

Recently Sigl (1997) studied numerically the behavior of $S_\sigma(\omega)$ for this case, using a phenomenological potential adapted to fit low-energy scattering data and deuteron properties. He found huge differences between the exact $S_\sigma(\omega)$ and the one derived in Born approximation. Put another way, because s -wave scattering dominates in this problem, the phase shifts are large and the Born approximation is not justified. For the chosen temperature and density, processes of the form $p+n \rightarrow d+\nu+\bar{\nu}$ play a dominant role while below the deuteron binding energy ($|\omega| < 2.2 \text{ MeV}$) only free-free transitions contribute to $S_\sigma(\omega)$. In this regime Sigl finds that his numerical $S_\sigma(\omega)$ and the one derived from the

OPE potential in Born approximation agree surprisingly well—there must be compensating effects between a potential and an approximation which are separately unjustified.

Thus one may probably estimate the relative significance of the pn process by using the OPE Born expression. One finds for the squared matrix element if one takes $|C_A|$ to be the same for protons and neutrons (Raffelt & Seckel 1995)

$$\left[\left(\frac{\mathbf{q}^2}{\mathbf{q}^2 + m_\pi^2} \right)^2 + 2 \left(\frac{\mathbf{q}_*^2}{\mathbf{q}_*^2 + m_\pi^2} \right)^2 + 2 \frac{\mathbf{q}^2 \mathbf{q}_*^2 - (\mathbf{q} \cdot \mathbf{q}_*)^2}{(\mathbf{q}^2 + m_\pi^2)(\mathbf{q}_*^2 + m_\pi^2)} \right] \quad (18)$$

with all coefficients the same as in Eq. (16). In the limit of a vanishing pion mass the expression in square brackets of Eq. (16) reduces to $3 - \beta$ where β is a phase-space average of $3(\mathbf{q} \cdot \mathbf{q}_*)^2 / \mathbf{q}^2 \mathbf{q}_*^2$ which for nondegenerate neutrons is found to be $\beta \approx 1.31$. In the present case the expression in square brackets reduces to $5 - 2\beta/3$. If we take for β the same value as before we find that the pn squared matrix element is about 2.5 times as large as the nn one. For the np process the bremsstrahlung rate is proportional to the product of the densities $n_p n_n$, i.e. to $n_B^2/4$ for an equal mix of protons and neutrons. For pure neutrons it is also proportional to $n_B^2/4$ where the factor 1/4 now derives from the phase-space reduction for identical particles. Put another way, the relative importance of the two cases is indeed well estimated by a comparison of the squared matrix elements.

For our conditions of interest protons are relatively rare so that ignoring the pn process leads to an underestimate of the bremsstrahlung rate which is probably not larger than a few tens of percent. Therefore, the error made by considering a medium of neutrons alone partially compensates the error made by using the OPE potential in Born approximation. We are thus led to believe that the compound error of our approximations does not exceed a few tens of percent.

3.3. Generic Representation

The squared matrix element Eq. (16) involves a factor ω^{-2} which survives the nucleon phase-space integration and which, in fact, is a generic feature of any bremsstrahlung process (Raffelt 1996). Therefore, we will always write the lowest-order scattering kernel as

$$S_\sigma^{(1)}(\omega) = \frac{\Gamma_\sigma}{\omega^2} s(\omega/T) \quad (19)$$

where Γ_σ is what we call the “spin fluctuation rate” while $s(x)$ is a dimensionless, slowly varying function of order unity. The factorization between Γ_σ and $s(x)$ is not unique. We take Γ_σ such that $s(0) = 1$ when the neutrons are nondegenerate and when the pion mass

has been ignored in the matrix element, leading to (Raffelt and Seckel 1995)

$$\Gamma_\sigma = \frac{8\sqrt{2\pi} \alpha_\pi^2}{3\pi^2} \eta_*^{3/2} \frac{T^2}{m_N}. \quad (20)$$

In terms of the neutron Fermi momentum p_F the “effective degeneracy parameter” is

$$\eta_* \equiv \frac{p_F^2}{2m_N T}; \quad (21)$$

it varies relatively little throughout a SN core and thus is a convenient measure of the neutron density. All modifications of $S_\sigma^{(1)}(\omega)$ by neutron degeneracy and the finite pion mass are included in the dimensionless function $s(x)$ which will be determined in Sec. 4.

For bremsstrahlung processes the singular behavior of $S_\sigma^{(1)}(\omega)$ at $\omega = 0$ is of no concern because it is suppressed by a sufficiently high power of ω in all relevant neutrino phase-space integrations. However, we want a kernel which consistently describes bremsstrahlung *and* the “inelasticity” of scattering. Even in this case the singularity can be interpreted under a phase-space integral such that one obtains finite and meaningful results (Sawyer 1995; Raffelt, Seckel & Sigl 1996). Still, the singular behavior is an artifact of the lowest-order perturbative expansion. Multiple-scattering effects (or formally a resummation of the neutron propagator) render $S_\sigma(\omega)$ a well-behaved function everywhere.

The interpretation of $S_\sigma(\omega)$ as a spin autocorrelation function suggests a phenomenological inclusion of multiple-scattering effects by the ansatz

$$S_\sigma(\omega) = \frac{\Gamma_\sigma}{\omega^2 + \Gamma^2/4} s(\omega/T). \quad (22)$$

In the classical limit of “hard collisions” one has $s(x) = 1$ and $\Gamma = \Gamma_\sigma$, leading to the correct normalization. In the general case we choose Γ such that $S_\sigma(\omega)$ is properly normalized.

To summarize, our scattering kernel is determined by a two-step procedure. We first calculate the perturbative $S_\sigma^{(1)}(\omega)$ by what amounts to a bremsstrahlung calculation and from which we extract $s(x)$. Next, we determine Γ in Eq. (22) such that the normalization Eq. (15) is fulfilled. We stress that the exact shape of $S_\sigma(\omega)$ around $\omega = 0$ is not crucial; in that sense our Lorentzian ansatz is well-motivated but arbitrary. The important quality of our ansatz is that it gives the correct normalization and thus the correct neutrino scattering cross section.

3.4. Neutrino Processes

3.4.1. Boltzmann Collision Integral

We have defined the scattering kernel essentially as the squared matrix element of a neutrino-nucleon process with the nucleon degrees of freedom integrated out. In order to calculate quantities like a neutrino mean free path it remains to integrate over the neutrino phase space. To this end we begin with the Boltzmann collision integral for neutrinos

$$\begin{aligned} \dot{f}_1|_{\text{coll}} = & C_A^2 G_F^2 n_B \int \frac{d^3 \mathbf{k}_2}{(2\pi)^3} (3 - \cos \theta) \\ & \times \left[(1 - f_1)(1 - \bar{f}_2) S_\sigma(-\omega_1 - \omega_2) - f_1 \bar{f}_2 S_\sigma(\omega_1 + \omega_2) \right. \\ & \left. + (1 - f_1) f_2 S_\sigma(-\omega_1 + \omega_2) - f_1 (1 - f_2) S_\sigma(\omega_1 - \omega_2) \right], \end{aligned} \quad (23)$$

where $f_{1,2}$ are now the occupation numbers of neutrinos with momenta \mathbf{k}_1 and \mathbf{k}_2 , respectively, while $\bar{f}_{1,2}$ are those of antineutrinos with the corresponding momenta. The first two terms in square brackets represent pair emission and pair absorption by the medium, i.e. the bremsstrahlung process and its inverse, while the third and fourth term represent the gain and loss terms from neutrino scattering on the nuclear medium. An analogous equation obtains for antineutrinos, i.e. for \bar{f}_1 .

For a practical numerical implementation we mention that the dimension of S_σ is (energy)⁻¹ so that an integral $\int d\omega S_\sigma(\omega)$ is a dimensionless number. Further, in natural units we may write $d^3 \mathbf{k}_2 = d\Omega_2 \omega_2^2 d\omega_2$ so that in the units usually employed in SN physics the integral expression in Eq. (23) has the dimension MeV². In the overall coefficient we write the baryon density as $n_B = \rho/m_N$ in terms of the mass density and the vacuum nucleon mass. Then the overall coefficient is numerically $C_A^2 G_F^2 n_B = 3.79 \times 10^4 \text{ s}^{-1} \text{ MeV}^{-2} \rho_{14}$, where $\rho_{14} = \rho/10^{14} \text{ g cm}^{-3}$ and where we have used $C_A = -1.26/2$.

3.4.2. Bremsstrahlung

To illustrate the use of the scattering kernel and for later reference we turn to a few simple quantities related to bremsstrahlung. The inverse mean free path of a neutrino with energy ω_1 against pair-absorption is

$$\lambda_1^{-1} = C_A^2 G_F^2 n_B \int \frac{d^3 \mathbf{k}_2}{(2\pi)^3} (3 - \cos \theta) \bar{f}_2 S_\sigma(\omega_1 + \omega_2) \quad (24)$$

with \bar{f}_2 the occupation number of the antineutrinos. We use a Maxwell-Boltzmann distribution at temperature T for the neutrinos. With the representation Eq. (19) for the

scattering kernel the spectral average is

$$\Gamma_{\nu\bar{\nu}nn\rightarrow nn} = \langle \lambda_1^{-1} \rangle = \frac{3C_A^2 G_F^2}{\pi} n_B T^2 \frac{\Gamma_\sigma/T}{20\pi} \xi \quad (25)$$

with the “dimensionless mean free path”

$$\xi \equiv 5 \int_0^\infty dx_1 \int_0^\infty dx_2 e^{-x_1} e^{-x_2} \frac{x_1^2 x_2^2}{(x_1 + x_2)^2} s(x_1 + x_2). \quad (26)$$

Here, $x_1 \equiv \omega_1/T$ and $x_2 \equiv \omega_2/T$ are the dimensionless neutrino and antineutrino energies respectively and we have ignored multiple-scattering effects. One of the energy integrations can be done analytically so that

$$\xi = \frac{1}{6} \int_0^\infty dx x^3 e^{-x} s(x). \quad (27)$$

Taking $s(x) = 1$ leads to $\xi = 1$; for realistic conditions it is in the range 0.2–0.5 (Sec. 4.5).

Next we consider the energy-loss rate of a medium which is taken to be transparent to neutrinos so that one may ignore phase-space blocking effects,

$$\begin{aligned} Q_{nn\rightarrow nn\nu\bar{\nu}} &= C_A^2 G_F^2 n_B \int \frac{d^3\mathbf{k}_1}{(2\pi)^3} \frac{d^3\mathbf{k}_2}{(2\pi)^3} (3 - \cos\theta) (\omega_1 + \omega_2) S_\sigma(-\omega_1 - \omega_2) \\ &= \frac{C_A^2 G_F^2 n_B}{40\pi^4} \int_0^\infty d\omega \omega^6 e^{-\omega/T} S_\sigma(\omega). \end{aligned} \quad (28)$$

The production rate of neutrino pairs instead of the energy-loss rate is found by dropping the energy $\omega = (\omega_1 + \omega_2)$ in this expression.

In numerical SN codes it is sometimes useful to consider the differential energy production rate into the neutrino channel only, not counting the energy which goes into antineutrinos. Therefore, we must integrate over the $\bar{\nu}$ phase-space, ignoring for simplicity Pauli blocking effects,

$$\frac{dQ_{\text{brems}}}{d\omega_1} = \frac{3C_A^2 G_F^2 n_B}{4\pi^4} \omega_1^3 \int_{\omega_1}^\infty d\omega (\omega - \omega_1)^2 e^{-\omega/T} S_\sigma(\omega). \quad (29)$$

The integral over this quantity is half of $Q_{nn\rightarrow nn\nu\bar{\nu}}$ of Eq. (28) because we now measure only the energy carried away by the neutrino, ignoring that carried by the antineutrino. In proper units we have $C_A^2 G_F^2 n_B = 1.13 \times 10^{31} \text{ ergs cm}^{-3} \text{ s}^{-1} \text{ MeV}^{-6} \rho_{14}$.

In order to compare the efficiency of energy transfer of different processes it will turn out to be useful to consider the net transfer of energy between a neutron fluid at temperature T to a neutrino fluid at temperature T_ν . It is found to be

$$\Delta Q_{nn\leftrightarrow nn\nu\bar{\nu}} = \frac{C_A^2 G_F^2 n_B}{40\pi^4} \int_0^\infty d\omega \omega^6 (e^{-\omega/T} - e^{-\omega/T_\nu}) S_\sigma(\omega). \quad (30)$$

With $\Delta T = T - T_\nu$ and in the limit $|\Delta T| \ll T$ this is

$$\begin{aligned} \frac{\Delta Q_{nn\leftrightarrow nn\nu\bar{\nu}}}{\Delta T} &= \frac{C_A^2 G_F^2 n_B}{40\pi^4} \frac{1}{T^2} \int_0^\infty d\omega \omega^7 e^{-\omega/T} S_\sigma(\omega) \\ &\simeq \frac{3C_A^2 G_F^2 n_B T^4}{\pi^4} \Gamma_\sigma \int_0^\infty dx \frac{x^5 e^{-x}}{120} s(x), \end{aligned} \quad (31)$$

where we have used the representation Eq. (19) for the lowest-order scattering kernel which may be used because the high power of ω appearing under the integral renders the low- ω modification by multiple-scattering irrelevant. With $s(x) = 1$ the integral is 1.

3.4.3. Neutrino Scattering

When studying the bremsstrahlung process one is naturally led to the Boltzmann collision integral of Eq. (23) which would be incomplete without the scattering processes. For a neutrino of energy ω_1 the scattering cross section differential with regard to the final-state energy ω_2 and the scattering angle is easily identified to be

$$\frac{d\sigma_1}{d\omega_2 d\Omega_2} = \frac{3 - \cos\theta}{4\pi} \frac{C_A^2 G_F^2}{\pi} \omega_2^2 \frac{S_\sigma(\omega_1 - \omega_2)}{2\pi}. \quad (32)$$

Numerically we have $C_A^2 G_F^2 = 2.10 \times 10^{-44} \text{ cm}^2 \text{ MeV}^{-2}$. If the medium is dilute so that the spin-fluctuation rate is small, then $S_\sigma(\omega)/2\pi$ is strongly peaked around $\omega = 0$ and actually must approach a δ -function which is normalized according to Eq. (15). Integrating over energy and angles then gives us the usual elastic scattering cross section $\sigma_1 = (3C_A^2 G_F^2/\pi)\omega_1^2$ which in a degenerate medium is reduced according to the right-hand side of Eq. (15).

Next we calculate the total axial-current cross section, averaged over a Maxwell-Boltzmann neutrino distribution. We find, in agreement with Raffelt & Seckel (1995),

$$\langle \sigma_A \rangle = \frac{3C_A^2 G_F^2}{\pi} 12T^2 \int_0^\infty d\omega \frac{12 + 6\omega/T + \omega^2/T^2}{12\pi} e^{-\omega/T} S_\sigma(\omega). \quad (33)$$

In the dilute limit where $S_\sigma(\omega) \rightarrow 2\pi\delta(\omega)$ the integral is 1. In general it is less than 1 because the function $S_\sigma(\omega)$ is normalized to 1 while the rest of the integrand falls monotonically with ω so that the integral has its maximum value when S_σ is narrowly peaked around $\omega = 0$. Therefore, NN interactions lead to a reduction of the average neutrino scattering cross section. This cross-section reduction is an unavoidable consequence of NN interactions and occurs on the same level of approximation as the bremsstrahlung emission or absorption of neutrino pairs.

In order to compare the efficiency of energy transfer of the “inelastic scattering process” with that of bremsstrahlung and other processes we finally consider the rate of energy transfer between a nucleon and a neutrino fluid at slightly different temperatures. We find

$$\frac{\Delta Q_{\nu nn \leftrightarrow nn\nu}}{\Delta T} = \frac{30 C_A^2 G_F^2 n_B T^4}{\pi^4} \Gamma_\sigma \int_0^\infty dx \frac{12 + 6x + x^2}{20} e^{-x} s(x), \quad (34)$$

where we have used Eq. (19) for the lowest-order scattering kernel. With $s(x) = 1$ the integral is 1.

4. Analytic Fitting Formula

4.1. General Representation

In order to represent the scattering kernel by analytic fitting formulae we write it in the form

$$S_\sigma(\omega) = \frac{1}{T} \frac{\gamma}{x^2 + (\gamma g/2)^2} s(x) \quad (35)$$

where $x = \omega/T$. The dimensionless quantities γ , g , and $s(x)$ depend on the medium density and temperature. We characterize the former by the neutron effective degeneracy parameter introduced in Eq. (21) which may be written as

$$\eta_* = \frac{(3\pi^2)^{2/3}}{2m_N T} \left(\frac{\rho}{m_N} \right)^{2/3} = 3.04 \rho_{14}^{2/3} T_{10}^{-1}. \quad (36)$$

The spin-fluctuation rate of Eq. (20) is numerically

$$\gamma \equiv \frac{\Gamma_\sigma}{T} = 1.63 \eta_*^{3/2} T_{10} = 8.6 \rho_{14} T_{10}^{-1/2}. \quad (37)$$

Both g and $s(x)$ are always of order unity so that simple estimates of bremsstrahlung-related quantities may be obtained by setting them both equal to 1.

The matrix element Eq. (16) involves the pion mass as one more dimensional parameter. It proves useful to express it in the form

$$y \equiv \frac{m_\pi^2}{m_N T} = 1.94 T_{10}^{-1}. \quad (38)$$

With this notation we have that the dimensionless scattering kernel $s(x)$ and the quantity g depend on the parameters y and η_* .

4.2. Nondegenerate Limit

We will construct a general analytic representation from an interpolation between the nondegenerate (ND) and degenerate (D) limiting cases. The former was treated by Raffelt & Seckel (1995); in a symmetric form their result can be expressed as

$$\begin{aligned} \bar{s}_{\text{ND}}(x, y) &\equiv \frac{s_{\text{ND}}(x, y) + s_{\text{ND}}(-x, y)}{2} = \\ &\frac{e^{-x/2} + e^{x/2}}{16} \int_{|x|}^{\infty} dt e^{-t/2} \frac{3x^2 + 6ty + 5y^2}{3} \left[\frac{2\sqrt{t^2 - x^2}}{x^2 + 2ty + y^2} - \frac{1}{t + y} \log \left(\frac{t + y + \sqrt{t^2 - x^2}}{t + y - \sqrt{t^2 - x^2}} \right) \right]. \end{aligned} \quad (39)$$

Evidently, this expression is even in x ; the structure function is recovered by $s_{\text{ND}}(x, y) = 2\bar{s}_{\text{ND}}(x, y)/(1 + e^{-x})$ and then obeys detailed balance. Its limiting behavior is

$$s_{\text{ND}}(x, y) = \begin{cases} 1 & \text{for } x = 0 \text{ and } y = 0, \\ (4\pi/x)^{1/2} & \text{for } x \gg 1 \text{ and } x \gg y, \\ \frac{80}{3} y^{-2} & \text{for } x = 0 \text{ and } y \gg 1, \end{cases} \quad (40)$$

i.e. it falls off to zero for either large x or y .

In order to construct an analytical fit we first extract the detailed-balance behavior explicitly by

$$s(x, y) = \hat{s}(x, y) \times \begin{cases} 1 & \text{for } x > 0, \\ e^{-x} & \text{for } x < 0. \end{cases} \quad (41)$$

An analytical fit for the $y = 0$ case (vanishing pion mass) is

$$\hat{s}_{y=0}(x) \simeq \left(\frac{x}{4\pi} + \left[1 + \left(12 + \frac{3}{\pi} \right) x \right]^{-1/12} \right)^{-1/2}. \quad (42)$$

This function reproduces the limiting behavior at $x = 0$ and $x \gg 1$, it has the correct derivative $1/2$ at $x = 0$, and it deviates from the correct result by no more than 2.5% anywhere. Likewise we have constructed

$$\hat{s}_{x=0}(y) \simeq \left[1 + \frac{y}{2} \log \left(\frac{y}{1 + y} \right) \right] \left[1 + \left(\frac{3y^2}{160} \right)^{4/9} \right]^{-9/4}. \quad (43)$$

It has the correct limiting behavior at $y = 0$ and $y \gg 1$, it is vertical at $y = 0$ in agreement with the full result, and its maximum error is below 4.5% anywhere. This function gives us a good idea of the suppression caused by including the pion mass.

A simple estimate of the compound scattering kernel is $\hat{s}_{\text{ND}}(x, y) \simeq \hat{s}_{y=0}(x) \hat{s}_{x=0}(y)$. However, it underestimates the correct value by as much as a factor of a few when both

x and y are a few which is the most relevant regime in a SN core. To construct a more suitable approximation we expand the square bracket in Eq. (39) in a power series in t and keep only the lowest term which is proportional to $t^{3/2}$. Now the exponential can be integrated so that

$$\hat{s}_{\text{ND}}(x, y) \simeq \frac{2\pi^{1/2}x^{3/2}(3x^2 + 6xy + 5y^2)}{3(x+y)^4}, \quad (44)$$

valid for $x \gg 1$ and $y \gg 1$. With a little bit of tinkering one can supplement it such that it behaves reasonably for small x and y ,

$$\hat{s}_{\text{ND}}(x, y) \simeq \frac{2\pi^{1/2} \left(x + 2 - e^{-y/12}\right)^{3/2} \left(x^2 + 2xy + \frac{5}{3}y^2 + 1\right)}{\pi^{1/2} + (\pi^{1/8} + x + y)^4}. \quad (45)$$

This function is 1 for $x = y = 0$ and has the correct limiting behavior for $y = 0$ and $x \gg 1$, but it does not have the correct limiting behavior for $x = 0$ and $y \gg 1$. The maximum error for any x is 14%, 7%, 5%, 9%, and 12% for $y = 0.5, 1, 2, 3,$ and 5 , respectively. The errors are even smaller for an integrated quantity like the average mean free path of Eq. (27) where we find a deviation of -4% , -1% , 4% , 7% and 10% for the same y values. This precision is good enough in view of the relatively crude treatment of the nuclear matrix element.

4.3. Degenerate Limit

In the degenerate limit the phase space integration can be carried out analytically even with a nonzero pion mass. Ishizuka & Yoshimura (1990) found

$$s_{\text{D}}(x, y, \eta_*) = 3 \left(\frac{\pi}{2}\right)^{5/2} \eta_*^{-5/2} \frac{(x^2 + 4\pi^2)x}{4\pi^2(1 - e^{-x})} f\left(\sqrt{\frac{y}{2\eta_*}}\right), \quad (46)$$

where

$$f(u) = 1 - \frac{5u}{6} \arctan\left(\frac{2}{u}\right) + \frac{u^2}{3(u^2 + 4)} + \frac{u^2}{6\sqrt{2u^2 + 4}} \arctan\left(\frac{2\sqrt{2u^2 + 4}}{u^2}\right). \quad (47)$$

The function $s_{\text{D}}(x)$ fulfills detailed balance explicitly. However, it is pathological in that it scales as x^3 for $x \gg 1$ which implies that the full scattering kernel is not normalizable in the sense of Eq. (15). Of course, the assumption of degenerate nucleons is never good for energy transfers which far exceed the nucleon Fermi energy. For $\omega \gg E_F$ ($x \gg E_F/T$) the full $s(x)$ must always approach $s_{\text{ND}}(x)$.

4.4. Interpolation

An interpolation which is accurate to within roughly 30–40% for all values of x and y is provided by

$$s = \left(\frac{1}{s_{\text{ND}}} + \frac{1}{s_{\text{D}}} \right)^{-1}. \quad (48)$$

One can do better by using

$$s = \left(s_{\text{ND}}^{-p(y)} + s_{\text{D}}^{-p(y)} \right)^{-1/p(y)} F(x, y, \eta_*) \left[1 + C(x, y, \eta_*) G(x, y, \eta_*) \right], \quad (49)$$

where

$$\begin{aligned} F(x, y, \eta_*) &= 1 + \frac{1}{[3 + (x - 1.2)^2 + x^{-4}] (1 + \eta_*^2) (1 + y^4)}, \\ G(x, y, \eta_*) &= 1 - 0.0044 x^{1.1} \frac{y}{0.8 + 0.06 y^{1.05}} \frac{\eta_*^{0.5}}{\eta_* + 0.2}, \\ C(x, y, \eta_*) &= \frac{1.1 x^{1.1} h(\eta_*)}{2.3 + h(\eta_*) x^{0.93} + 0.0001 x^{1.2}} \frac{30}{30 + 0.005 x^{2.8}}, \\ p(y) &= 0.67 + 0.18 y^{0.4}, \\ h(\eta_*) &= \frac{0.1 \eta_*}{2.39 + 0.1 \eta_*^{1.1}}. \end{aligned} \quad (50)$$

This interpolation function reproduces the true value of the scattering kernel to within 5–10% in the physically interesting parameter space, $y \simeq 2\text{--}6$ and $\eta_* \simeq 2\text{--}6$, and maximum deviations for any value of the parameters of less than 25%. As discussed in Sec. 3.3, the uncertainties from the nuclear matrix element are at least of that magnitude so that this fitting accuracy is entirely sufficient.

In Table 2 we give $s(x, y, \eta_*)$, both the numerically calculated values and for comparison the analytical fit. In Fig. 3 we plot $s(x)$ for different values of y and η_* where the solid lines represent the numerical result and the short-dashed ones the fitting formula. The detailed-balance condition tells us that $s(-x) = s(x)e^{-x}$. Still, we plot $s(x)$ somewhat across $x = 0$ in order to illustrate that it is smooth at the origin. In both panels the upper curve corresponds to a vanishing pion mass ($y = 0$) and essentially nondegenerate conditions ($\eta_* = 0.31$).

The upper panel illustrates the effect of degeneracy which suppresses the scattering kernel at low x , but enhances it at large ones. All of these curves approach the nondegenerate case asymptotically in the limit $x \rightarrow \infty$, but they do so from above. The lower panel illustrates the impact of including the pion mass in the matrix element. It suppresses the scattering kernel at low x by an amount which depends on y , and again the curves approach the $y = 0$ case in the large x limit, however here they do so from below.

4.5. Multiple Scattering

It remains to determine the function $g(y, \eta_*)$ for the denominator of Eq. (35) which must be adjusted to meet the normalization condition Eq. (15),

$$\int_{-\infty}^{+\infty} \frac{dx}{2\pi} \frac{\gamma}{x^2 + (\gamma g/2)^2} s(x) = B. \quad (51)$$

For ND conditions and when $\gamma \ll 1$ the Lorentzian is essentially a δ function and we have for the integral $s_{\text{ND}}(0)/g$. Therefore, in the limit $y = 0$ and $\eta_* = 0$, which also implies $\gamma = 0$, we have $g = 1$ because γ was defined such that in this limit $s_{\text{ND}}(0) = 1$.

We have determined the function $g(y, \eta_*)$ using the normalization condition Eq. (15) and our analytic approximation formula Eq. (49) for $s(x)$. Furthermore we need to provide an analytic approximation for $g(y, \eta_*)$ that can be implemented in numerical calculations. For very high values of y , we know that $g \propto y^{-2}$ and for $y \rightarrow 0$ we know that $g \rightarrow 0.5$ in the degenerate limit and $g \rightarrow 1$ in the nondegenerate limit. A decent analytic fit that has the correct limiting behavior is given by

$$g(y, \eta_*) = \frac{\alpha_1 + \alpha_2 y^{p_1}}{1 + \alpha_3 y^{p_2} + \alpha_2 y^{p_1+2}/13.75}, \quad (52)$$

where the coefficients are given by

$$\begin{aligned} \alpha_1 &= \frac{0.5 + \eta^{-1}}{1 + \eta^{-1}} \frac{1}{25 y^2 + 1} + (0.5 + \eta/15.6) \frac{25 y^2}{25 y^2 + 1}, \\ \alpha_2 &= \frac{0.63 + 0.04 \eta^{1.45}}{1 + 0.02 \eta^{2.5}}, \\ \alpha_3 &= 1.2 \exp(0.6 \eta - 0.4 \eta^{1.5}), \\ p_1 &= \frac{1.8 + 0.45 \eta}{1 + 0.15 \eta^{1.5}}, \\ p_2 &= 2.3 - \frac{0.05 \eta}{1 + 0.025 \eta}. \end{aligned} \quad (53)$$

In Fig. 4 we show $g(y, \eta_*)$ as a function of y for different values of the degeneracy parameter η_* (solid lines) as well as our analytic fit to $g(y, \eta_*)$ (dashes). Also, in Fig. 5 we show the normalization $B(\eta_*)$ which was defined in Eq. (15) as a function of η_* .

We may now calculate the average neutrino absorption rate in its dimensionless form Eq. (27). In Table 3 we give values for ξ based on our analytic approximation scheme, both with and without the inclusion of multiple-scattering effects. For realistic SN conditions where $y \simeq 2$ –6 and $\eta_* \simeq 2$ –6 we see that $\xi \simeq 0.2$ –0.5. Multiple scattering is not a strong effect for the average absorption rate.

However, to calculate inelastic scattering it is unavoidable to include the multiple scattering effect. With our function $g(y, \eta_*)$ the scattering kernel is self-consistent in that it allows for the simultaneous treatment of bremsstrahlung and inelastic scattering while reproducing the correct total scattering cross section.

5. Conclusions

We have studied the neutron-neutron bremsstrahlung process $nn \leftrightarrow nn\nu\bar{\nu}$ as an opacity source for neutrinos and its impact on the neutrino spectra formation in supernovae. For ν_μ and ν_τ , bremsstrahlung is by far the most important number-changing reaction, far more important than e^+e^- annihilation or the plasma process. As an energy-changing process it is roughly as strong as elastic scattering on electrons and positrons. We estimate that including bremsstrahlung will reduce the ν_μ temperature by more than 1 MeV. This is only a differential effect in the sense that the ν_μ and $\bar{\nu}_e$ spectral temperatures become closer by this amount. Their absolute changes can not be determined by our simple procedure. The overall magnitude of our differential effect is in agreement with Suzuki’s (1991, 1993) numerical simulations.

If one includes the bremsstrahlung process it is inconsistent to ignore the inelasticity of νn scattering which may be pictured as the “crossed bremsstrahlung process” $\nu nn \rightarrow nn\nu$. This process cannot change the neutrino number density, but as a source of spectral equilibration it is roughly a factor of 10 more important than bremsstrahlung and thus also far more important than νe scattering. Moreover, depending on details of the temperature and density profile of the SN core surface layers, the nucleon recoil in νN collisions is of roughly equal importance to the inelasticity (Janka et al. 1996). Bremsstrahlung, inelastic scattering, and recoils near the neutrino spheres is likely to make the spectra and fluxes of the different neutrino species far more similar than had been thought previously. This would modify all phenomena related to neutrino flavor oscillations which rely on the difference in the spectral temperatures to be effective.

The main purpose of our paper was to provide an explicit form for the scattering kernel $S_\sigma(\omega)$ that will allow one to study the impact of bremsstrahlung and inelastic scattering consistently in a numerical simulation.

Our derivation is fundamentally perturbative; it is useful to study the spectra formation in the surface layers of a proto neutron star. We believe our scattering kernel to be appropriate for densities roughly below $10^{14} \text{ g cm}^{-3}$. At higher densities our result predicts a huge suppression of the total νN scattering cross section which opens the thorny

issue of its actual magnitude. This problem has not been solved so that any SN simulation has to rely on an arbitrary prescription for the neutrino diffusion coefficients in the deep interior. The SN 1987A signal (Keil, Janka & Raffelt 1995) as well as the f -sum rule for the spin-density structure function (Sigl 1996) indicate that the cross-section suppression is not as large as predicted by our scattering kernel, but how large the cross sections truly are is not known. Recent attempts to include the correct nucleon dispersion relation as well as hyperons (Reddy & Prakash 1997) predict modifications of the “standard cross sections” by factors of order unity, but no attempt was made to address the modifications caused by the inevitable nucleon or hyperon spin-spin interactions.

Another shortcoming of our scattering kernel is that it does not include recoil effects. In some regions of a SN core it may be even more effective than NN interactions at modifying the neutrino energy in a collision. A scattering kernel which includes recoils and NN interactions simultaneously requires avoiding the long-wavelength approximation, a rather complicated task that would imply another variable (the scattering angle) explicitly in the scattering kernel.

Our estimates clearly show that bremsstrahlung and its related processes cannot be ignored for the formation of the neutrino spectra in a SN core. However, to determine the real magnitude of the modification one needs to perform a self-consistent numerical analysis which includes feedback effects on the medium. If such a study reveals that the modifications are as severe as suggested by our estimates one may be motivated to derive a more complete perturbative scattering kernel. One could study the proton-neutron process on the basis of a realistic nucleon-nucleon potential in the spirit of Sigl’s (1997) recent work, thereby avoiding the pathologies inherent in an OPE Born treatment of np scattering. Moreover, it would be cumbersome but straightforward to include recoil effects and NN interactions simultaneously in the scattering kernel. Unfortunately, it remains far from obvious how to proceed extending the scattering kernel into the high-density regime.

Acknowledgements

We thank Thomas Janka and Adam Burrows for invaluable comments on early versions of the manuscript and Wolfram Weise for discussions about the use of the one-pion exchange potential. We are especially indebted to David Seckel for prodding us to include a discussion of inelastic scattering and recoils. Our research was supported, in part, by the European Union under contract No. CHRX CT930120, by the Deutsche Forschungsgemeinschaft under grant No. SFB 375, and by the Theoretical Astrophysics Center under the Danish National Research Council.

A. Nucleon Phase-Space Integration

We give some details of solving the nucleon phase-space integral Eq. (14). From the original 12-dimensional integral one can integrate out 8 dimensions analytically so that in the end only a four dimensional integral remains to be done numerically. First, the three-dimensional momentum delta function is used to integrate out $d^3\mathbf{p}_4$. Because the nucleons are nonrelativistic their energy is $E_i = p_i^2/2m_N$ so that

$$E_1 + E_2 - E_3 - E_4 + \omega = \frac{-2p_3^2 - 2\mathbf{p}_1 \cdot \mathbf{p}_2 + 2\mathbf{p}_1 \cdot \mathbf{p}_3 + 2\mathbf{p}_2 \cdot \mathbf{p}_3}{2m_N} + \omega. \quad (\text{A1})$$

Because of the assumed isotropy of the medium the \mathbf{p}_1 momentum may be chosen in the z -direction, i.e. we have trivially $\int d^3\mathbf{p}_1 = 4\pi \int dp_1$ with $p_1 = |\mathbf{p}_1|$. Next we use polar coordinates with α and β the polar and azimuthal angles of \mathbf{p}_2 relative to \mathbf{p}_1 and θ and ϕ those of \mathbf{p}_3 so that

$$d^3\mathbf{p}_2 = p_2^2 dp_2 d\cos\alpha d\beta \quad (\text{A2})$$

$$d^3\mathbf{p}_3 = p_3^2 dp_3 d\cos\theta d\phi. \quad (\text{A3})$$

Because of the medium's isotropy one of the azimuthal integrations is trivial. We chose the $d\phi$ integration so that three nontrivial angular integrations remain. In terms of these remaining angular variables we have

$$\mathbf{p}_1 \cdot \mathbf{p}_2 = p_1 p_2 \cos\alpha \quad (\text{A4})$$

$$\mathbf{p}_1 \cdot \mathbf{p}_3 = p_1 p_3 \cos\theta \quad (\text{A5})$$

$$\mathbf{p}_2 \cdot \mathbf{p}_3 = p_2 p_3 \cos\alpha \cos\theta + \sin\alpha \sin\theta \cos\beta. \quad (\text{A6})$$

The integration over $d\beta$ is carried out using the δ -function where we write $f(\beta) \equiv E_1 + E_2 - E_3 - E_4 + \omega$ so that

$$\int_0^{2\pi} d\beta \delta(f(\beta)) = \sum_i \int_0^{2\pi} d\beta \frac{1}{\left| \frac{df(\beta)}{d\beta} \right|_{\beta=\beta_i}} \delta(\beta - \beta_i), \quad (\text{A7})$$

where β_i with $i = 1, 2$ are the two roots of $f(\beta) = 0$, one in the interval $[0, \pi]$ and one in the interval $[\pi, 2\pi]$. Because Eq. (A7) is symmetric in β it is enough to use β_1 which is in the interval $[0, \pi]$ and multiply by 2. Thus we end up with

$$\int_0^{2\pi} d\beta \delta(f(\beta)) = \frac{2}{\left| \frac{df(\beta)}{d\beta} \right|_{\beta=\beta_1}} \Theta \left(\left| \frac{df(\beta)}{d\beta} \right|_{\beta=\beta_1}^2 \right). \quad (\text{A8})$$

The derivative may be written in the form

$$\left| \frac{df(\beta)}{d\beta} \right|_{\beta=\beta_1} = \sqrt{az^2 + bz + c}, \quad (\text{A9})$$

where $z \equiv \cos \alpha$ and

$$\begin{aligned} a &= p_2^2(-p_1^2 - p_3^2 + 2p_1p_3 \cos \theta), \\ b &= 2\omega m_N p_1 p_2 - 2p_1 p_2 p_3^2 - 2\omega m_N p_2 p_3 \cos \theta + 2p_1^2 p_2 p_3 \cos \theta \\ &\quad + 2p_2 p_3^3 \cos \theta - 2p_1 p_2 p_3^2 \cos^2 \theta, \\ c &= \omega^2 m_N^2 + 2\omega m_N p_3^2 + p_2^2 p_3^2 - p_3^4 - 2\omega m_N p_1 p_3 \cos \theta \\ &\quad + 2p_1 p_3^3 \cos \theta - p_1^2 p_3^2 \cos^2 \theta - p_2^2 p_3^2 \cos^2 \theta. \end{aligned} \quad (\text{A10})$$

The integration of the δ function also fixes $E_4 = E_1 + E_2 - E_3 + \omega$ which is used to determine the Pauli-blocking factor of particle 4 in the phase-space integral.

In order to perform the integration over $dz = d \cos \alpha$ analytically we note that partial integrations allow us to reduce the integrand to a sum of two terms. One of them is independent of z while the other is of the form $1/(qz + r)$ where q and r are expressions which do not depend on z . We find explicitly

$$\begin{aligned} \int_{-\infty}^{+\infty} \frac{dz}{\sqrt{az^2 + bz + c}} \Theta(az^2 + bz + c) &= \frac{\pi}{\sqrt{-a}} \Theta(b^2 - 4ac), \\ \int_{-\infty}^{+\infty} \frac{dz}{\sqrt{az^2 + bz + c}} \frac{1}{qz + r} \Theta(az^2 + bz + c) &= \frac{\pi \Theta(b^2 - 4ac)}{\sqrt{-ar^2q^{-2} + brq^{-1} - c}}. \end{aligned} \quad (\text{A11})$$

The step function in the integrand singles out the physically relevant range where $-1 \leq z \leq +1$.

After these analytic manipulations we are left with a four dimensional numerical integral over $dp_1 dp_2 dp_3 d \cos \theta$ where the integration region is determined by the step function $\Theta(b^2 - 4ac)$.

REFERENCES

- Blatt, J. M. & Weisskopf, V. F. 1979, *Theoretical Nuclear Physics*, (Springer-Verlag New York)
- Burrows, A., & Mazurek, T. J. 1982, *Ap. J.*, 259, 330
- Burrows, A., & Mazurek, T. J. 1983, *Nature*, 301, 315
- Choi, K., Kang, K., & Kim, J. E. 1989 *Phys. Rev. Lett.*, 62, 849.
- Ericson, T., & Mathiot, J.-F. 1989, *Phys. Lett. B*, 219, 507
- Ericson, T., & Weise, W. 1988, *Pions and Nuclei* (Clarendon Press, Oxford)
- Friman, B. L., & Maxwell, O. V. 1979, *Ap. J.*, 232, 541
- Ishizuka, N., & Yoshimura, M. 1990, *Prog. Theor. Phys.*, 84, 233
- Janka, H.-T 1991, Ph.D. Thesis, Technische Universität München, Report No. MPA-587 (unpublished).
- Janka, H.-T., Keil, W., Raffelt, G., & Seckel, D. 1996, *Phys. Rev. Lett.*, 76, 2621
- Keil, W. & Janka, H.-T 1995, *Astron. Astrophys.*, 296, 145
- Keil, W., Janka, H.-T & Müller, E. 1996, *Ap. J.*, 473, L111
- Keil, W., Janka, H.-T. & Raffelt, G. 1995, *Phys. Rev. D*, 51, 6635
- Raffelt, G. 1996, *Stars as Laboratories for Fundamental Physics* (University of Chicago Press, Chicago)
- Raffelt, G., & Seckel, D. 1995, *Phys. Rev. D*, 52, 1780
- Raffelt, G., Seckel, D., & Sigl, G. 1996, *Phys. Rev. D*, 54, 2784
- Raffelt, G., & Strobel, T. 1997, *Phys. Rev. D*, 55, 523
- Reddy, S., & Prakash, M. 1997, *Ap. J.*, 478, 689
- Sawyer, R. F. 1995, *Phys. Rev. Lett.*, 75, 2260
- Shapiro, S. L., & Teukolsky, S. A. 1983, *Black Holes, White Dwarfs, and Neutron Stars* (Wiley-Interscience)

Sigl, G. 1996, *Phys. Rev. Lett.*, 76, 2625

Sigl, G. 1997, *Phys. Rev. D*, 56, 3179

Suzuki, H. 1991, *Num. Astrophys. Japan*, 2, 267

Suzuki, H. 1993, in: *Frontiers of Neutrino Astrophysics*, Proc. of the Internat. Symp. on Neutrino Astrophys., Oct. 19–22, 1992, Takayama/Kamioka, Japan, ed. by Y. Suzuki and K. Nakamura (Universal Academy Press, Tokyo)

Tubbs, D. L. 1979, *Ap. J.*, 231, 846

Turner, M. S., Kang, H.-S., & Steigman, G. 1989, *Phys. Rev. D*, 40, 299

Table 1. Neutrino Energy Spheres

Flavor:	$\nu_\mu, \nu_\tau, \bar{\nu}_\mu, \bar{\nu}_\tau$					$\bar{\nu}_e$				
f_{brems}	0	1	5	10	20	0	1	5	10	20
$\rho_{\text{sph}} [10^{14} \text{ g/cm}^3]$	1.20	0.99	0.85	0.78	0.71	0.82	0.77	0.70	0.66	0.62
$T_{\text{sph}} [\text{MeV}]$	8.78	7.50	6.67	6.31	5.99	6.52	6.25	5.94	5.77	5.60
$T_{\text{sph}}^\infty [\text{MeV}]$	7.39	6.32	5.63	5.33	5.06	5.49	5.25	5.02	4.87	4.73
$\tau_{\text{sph}}^{\text{tot}}$	16.3	7.11	4.42	3.49	2.83	3.83	2.78	2.18	1.93	1.76

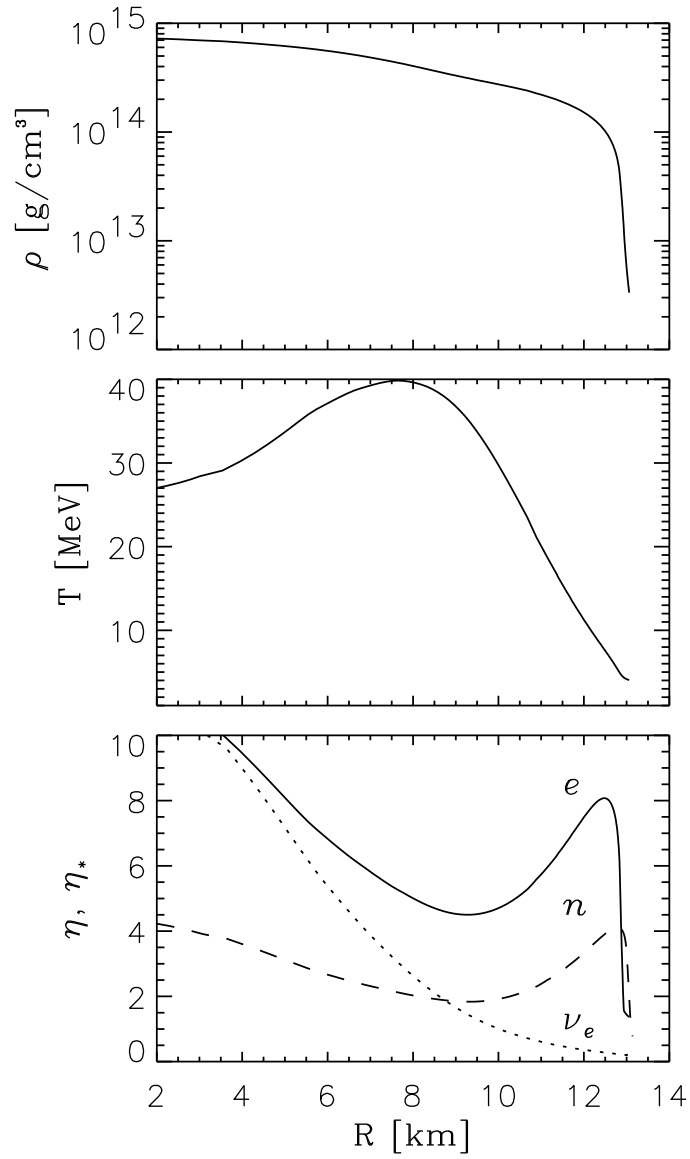


Fig. 1.— Physical parameters of the proto neutron star model S2BH₀ of Keil, Janka & Raffelt (1995) which represents a SN core 1 s after bounce. For the neutrons we show the effective degeneracy parameter η_* as defined in Eq. (21), taking the vacuum nucleon mass for m_N .

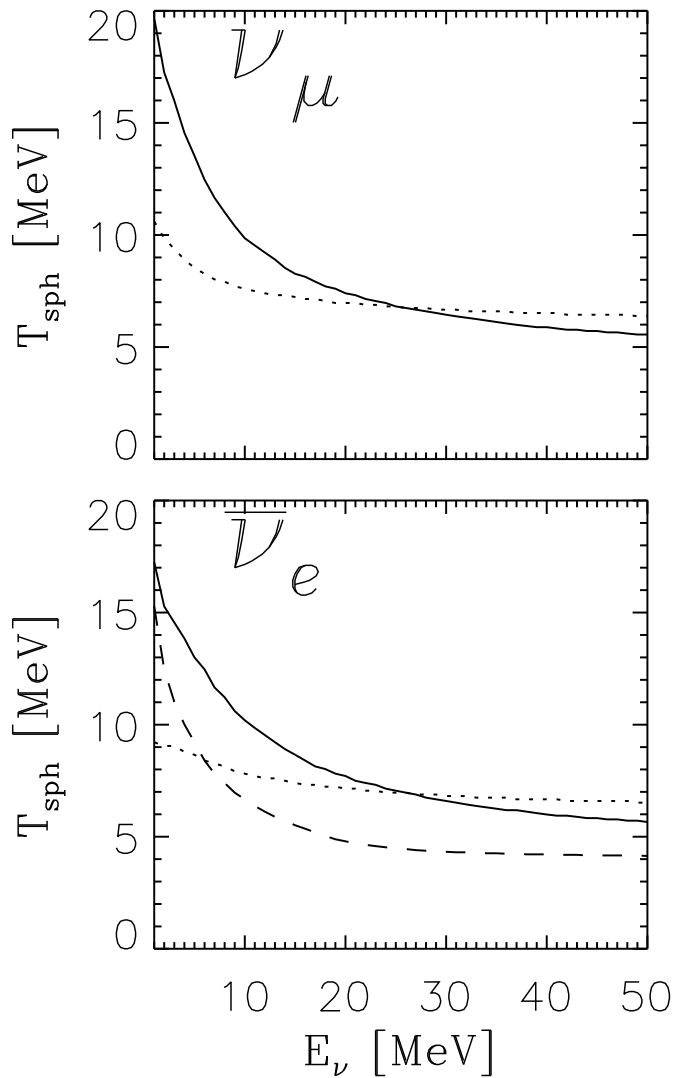


Fig. 2.— Temperature of the medium (SN model of Fig. 1) at last energy exchange for different processes: Scattering on e^\pm (solid line), inverse bremsstrahlung $\nu\bar{\nu}nn \rightarrow nn$ (short dashes), and β -absorption $\bar{\nu}_e p \rightarrow ne$ (long dashes).

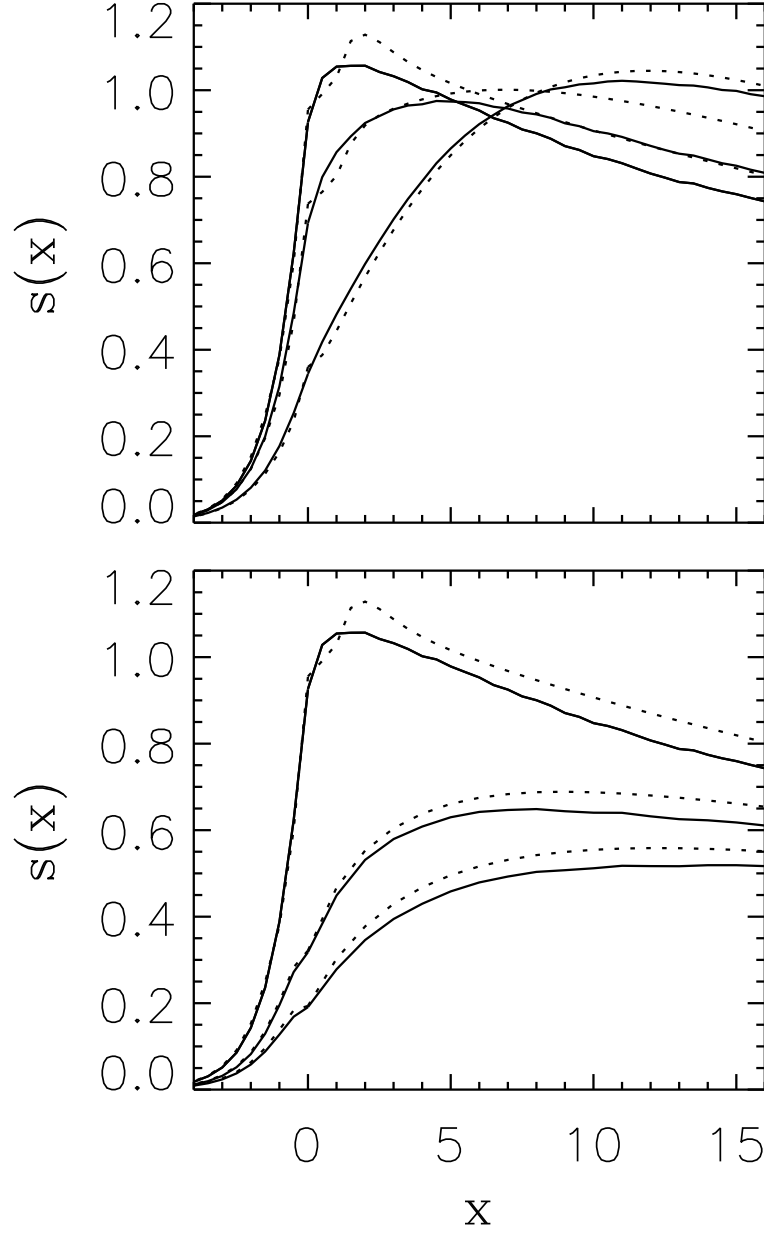


Fig. 3.— Dimensionless scattering kernel $s(x, y, \eta_*)$. *Upper Panel:* Pion mass ignored ($y = 0$) with $\eta_* = 0.31, 1.01,$ and 2.42 from top to bottom, corresponding to $\eta = -2, 0,$ and $2,$ respectively. The solid curves are numerical results whereas the short-dashed ones are the analytical approximation Eq. (49). *Lower Panel:* Nondegenerate case ($\eta = -2, \eta_* = 0.31$) with $y = 0, 2,$ and 4 from top to bottom.

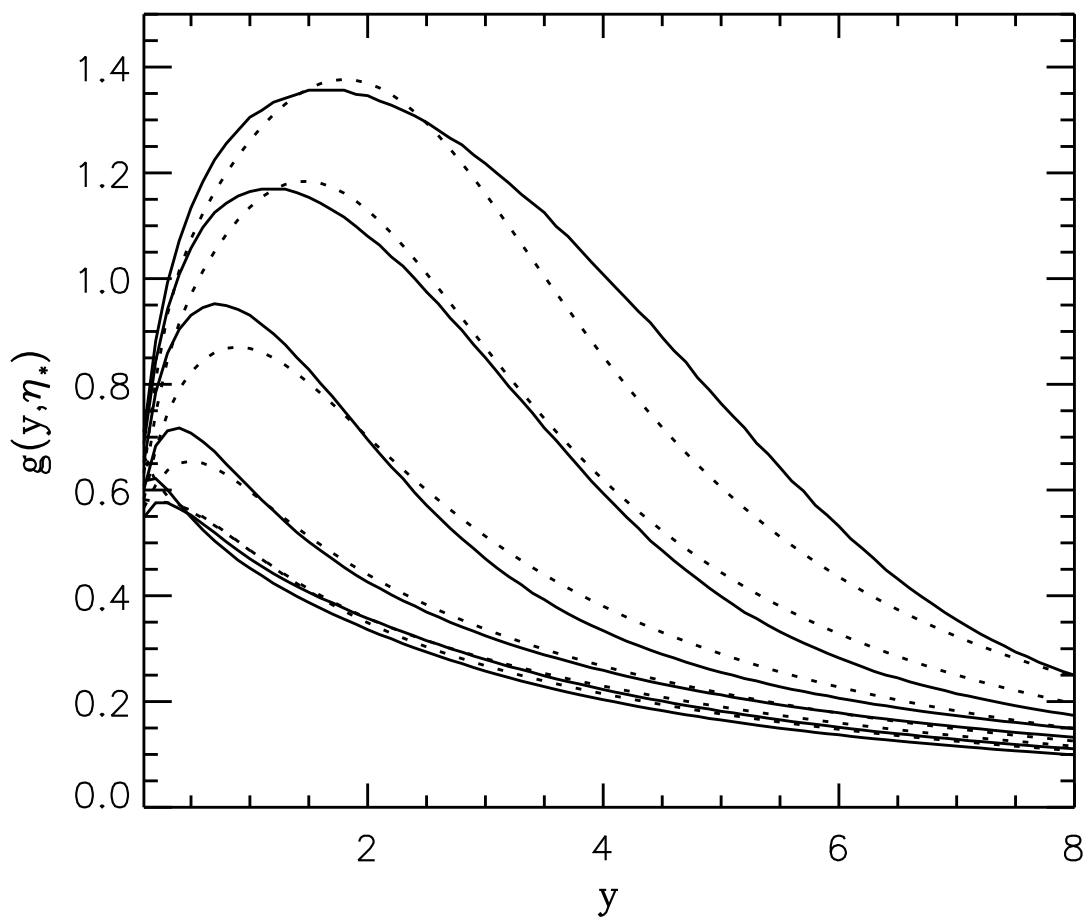


Fig. 4.— Function $g(y, \eta_*)$ as defined in Secs. 4.1 and 4.5 to take multiple-scattering effects into account. From bottom to top the curves are for $\eta_* = 0.31, 1.01, 2.42, 4.22, 6.14,$ and 8.11 respectively. The numerically calculated $g(y, \eta_*)$ are shown as full lines, whereas the analytic fit from Eq. (52) is represented by the dotted lines.

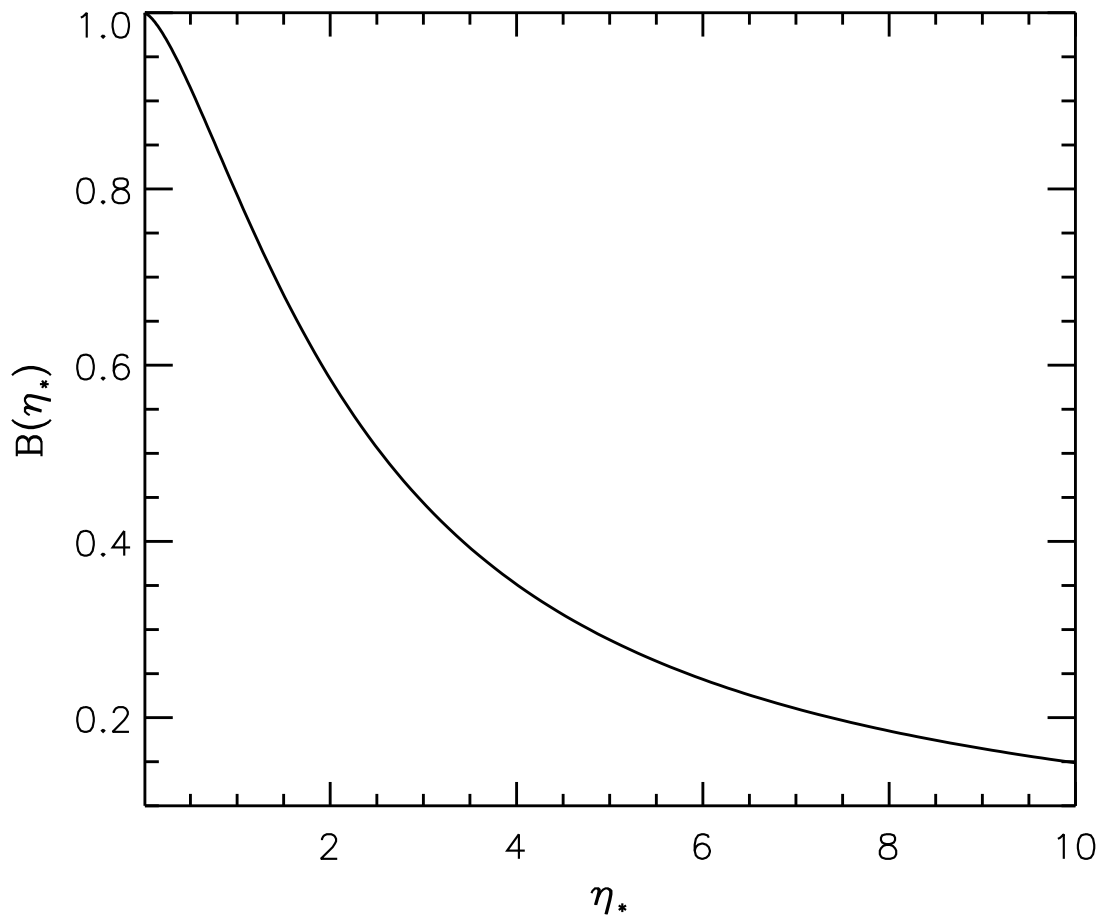


Fig. 5.— The normalization function $B(\eta_*)$ defined in Eq. (15) as a function of the nucleon degeneracy parameter η_* .

Table 2. $s(x, y, \eta_*)$ in the form “Numerical Value/Analytical Approximation”.

$y =$	0	2	4	6	8
$\eta = 0 \quad (\eta_* = 1.01)$					
$x = 0$	0.701/0.735	0.267/0.277	0.166/0.171	0.117/0.117	0.088/0.086
1	0.861/0.799	0.389/0.412	0.248/0.272	0.177/0.193	0.134/0.145
2	0.926/0.916	0.482/0.508	0.321/0.352	0.233/0.259	0.179/0.198
3	0.959/0.955	0.551/0.579	0.381/0.416	0.284/0.314	0.222/0.246
4	0.973/0.977	0.600/0.633	0.429/0.466	0.327/0.360	0.259/0.287
5	0.976/0.991	0.636/0.673	0.467/0.506	0.362/0.398	0.291/0.322
6	0.971/0.998	0.660/0.702	0.496/0.538	0.391/0.429	0.319/0.351
7	0.959/1.000	0.675/0.724	0.518/0.562	0.414/0.454	0.341/0.375
8	0.945/0.998	0.685/0.738	0.534/0.581	0.433/0.474	0.360/0.395
9	0.928/0.993	0.690/0.748	0.546/0.595	0.448/0.489	0.376/0.411
10	0.911/0.985	0.691/0.753	0.554/0.605	0.459/0.501	0.389/0.424
$\eta = 2 \quad (\eta_* = 2.42)$					
$x = 0$	0.349/0.360	0.165/0.172	0.111/0.115	0.082/0.084	0.064/0.064
1	0.485/0.443	0.252/0.270	0.172/0.190	0.128/0.141	0.101/0.110
2	0.600/0.567	0.342/0.368	0.240/0.267	0.182/0.203	0.144/0.160
3	0.705/0.676	0.431/0.463	0.310/0.343	0.238/0.266	0.191/0.212
4	0.794/0.770	0.513/0.550	0.378/0.415	0.295/0.326	0.238/0.263
5	0.867/0.847	0.585/0.624	0.440/0.478	0.349/0.381	0.285/0.311
6	0.924/0.909	0.646/0.685	0.495/0.532	0.397/0.429	0.328/0.353
7	0.964/0.957	0.694/0.735	0.541/0.577	0.439/0.469	0.366/0.390
8	0.993/0.992	0.733/0.773	0.580/0.613	0.476/0.502	0.400/0.421
9	1.011/1.016	0.763/0.801	0.611/0.641	0.506/0.529	0.428/0.446
10	1.020/1.032	0.784/0.821	0.636/0.663	0.531/0.550	0.453/0.466
$\eta = 4 \quad (\eta_* = 4.22)$					
$x = 0$	0.153/0.154	0.086/0.087	0.063/0.064	0.049/0.050	0.040/0.040
1	0.229/0.219	0.136/0.145	0.100/0.109	0.078/0.086	0.064/0.070
2	0.313/0.312	0.197/0.218	0.147/0.167	0.117/0.133	0.096/0.109
3	0.408/0.415	0.269/0.304	0.204/0.235	0.163/0.189	0.135/0.156
4	0.509/0.522	0.349/0.396	0.269/0.310	0.217/0.252	0.181/0.209
5	0.613/0.625	0.434/0.489	0.339/0.387	0.276/0.316	0.231/0.263
6	0.712/0.720	0.518/0.577	0.409/0.460	0.337/0.378	0.284/0.317
7	0.803/0.802	0.598/0.654	0.478/0.525	0.397/0.434	0.336/0.366
8	0.884/0.871	0.671/0.720	0.543/0.582	0.454/0.484	0.387/0.410
9	0.953/0.927	0.736/0.773	0.602/0.629	0.506/0.525	0.435/0.447
10	1.011/0.970	0.793/0.814	0.654/0.667	0.554/0.559	0.478/0.477

Table 2—Continued

$y =$	0	2	4	6	8
$\eta = 6 \quad (\eta_* = 6.14)$					
$x = 0$	0.074/0.074	0.046/0.046	0.036/0.036	0.029/0.029	0.025/0.025
1	0.114/0.116	0.074/0.080	0.057/0.063	0.047/0.052	0.040/0.044
2	0.164/0.177	0.111/0.127	0.087/0.101	0.072/0.084	0.061/0.071
3	0.227/0.253	0.159/0.189	0.126/0.152	0.104/0.126	0.088/0.107
4	0.300/0.340	0.217/0.265	0.173/0.214	0.144/0.179	0.123/0.152
5	0.385/0.435	0.284/0.350	0.229/0.284	0.192/0.238	0.165/0.203
6	0.476/0.530	0.359/0.438	0.293/0.359	0.247/0.301	0.212/0.258
7	0.572/0.621	0.440/0.526	0.361/0.432	0.306/0.364	0.264/0.313
8	0.669/0.705	0.522/0.606	0.432/0.501	0.368/0.424	0.319/0.364
9	0.763/0.779	0.603/0.678	0.503/0.563	0.431/0.477	0.375/0.411
10	0.851/0.841	0.681/0.738	0.572/0.615	0.492/0.523	0.431/0.452
$\eta = 8 \quad (\eta_* = 8.11)$					
$x = 0$	0.043/0.041	0.029/0.027	0.023/0.022	0.020/0.018	0.017/0.016
1	0.068/0.068	0.046/0.048	0.037/0.039	0.031/0.033	0.027/0.029
2	0.100/0.108	0.071/0.079	0.057/0.065	0.048/0.055	0.042/0.048
3	0.142/0.161	0.103/0.122	0.084/0.101	0.072/0.086	0.062/0.074
4	0.194/0.227	0.145/0.178	0.119/0.147	0.102/0.126	0.088/0.109
5	0.257/0.302	0.196/0.246	0.163/0.204	0.139/0.175	0.121/0.152
6	0.331/0.385	0.257/0.322	0.214/0.269	0.184/0.230	0.161/0.201
7	0.413/0.469	0.325/0.403	0.273/0.338	0.236/0.290	0.207/0.253
8	0.503/0.552	0.401/0.484	0.339/0.408	0.294/0.351	0.259/0.306
9	0.597/0.630	0.482/0.561	0.409/0.474	0.356/0.409	0.315/0.357
10	0.693/0.700	0.566/0.631	0.483/0.535	0.422/0.462	0.374/0.404

Table 3. Dimensionless mean free path against pair-absorption ξ as defined in Eq. (27). Values are given as “without/with” multiple scattering.

$\eta_* =$	1	2	4	6	8
$y = 1$	0.750/0.712	0.666/0.488	0.471/0.102	0.321/0.017	0.222/0.005
2	0.609/0.604	0.557/0.524	0.408/0.237	0.284/0.052	0.199/0.013
4	0.447/0.447	0.417/0.415	0.320/0.297	0.230/0.157	0.166/0.063
6	0.345/0.345	0.327/0.327	0.259/0.256	0.192/0.179	0.141/0.112
8	0.276/0.276	0.264/0.264	0.215/0.215	0.164/0.161	0.123/0.116